![JTMAE — The Journal of Technology, Management, and Applied Engineering]

Vijai M. Moorthy
Department of Electronic Engineering, Howard College, University of KwaZulu-Natal, Durban, South Africa

Viranjay M. Srivastava
Department of Electronic Engineering, Howard College, University of KwaZulu-Natal, Durban, South Africa

Geometrical Optimization and Simulation of NPDA Device for Future Use in Retinal Implant

Keywords:
Photodiode; Nano Photodiode Array; Optimization; Modeling; Subretinal Prostheses; Nanomaterial

EMPIRICAL RESEARCH

Dr. VIJAI M. MOORTHY

(Member, IEEE) was born in Karaikudi, Tamil Nadu, India, in 1986. He received a bachelor's degree B.Tech in Computer Science and engineering in 2008, a master's degree M.Tech in VLSI design in 2010 from SASTRA University, and a Ph.D. degree in the field of BioMEMS and MEMS design in 2021 from Annamalai University, Tamil Nādu.

He has worked on the fabrication of devices and the development of biomedical and Nano-electronic devices. He is currently a Postdoctoral Research Scholar with the Dept. EE, Howard College, University of KwaZulu-Natal, Durban, South Africa. He has more than 12 years of teaching and research experience in the area of VLSI design, MEMS, Bio-devices, and Nanomaterials. He has authored and co-authored more than 30 technical offerings, including articles in international refereed journals, book chapters, and international/national conferences. He is a Reviewer in IET MNL journal.

Geometrical Optimization and Simulation of NPDA Device for Future Use in Retinal Implant

ABSTRACT

The focus of this research was to improve the device structure and electrode geometry of nano photodiode array (NPDA) subretinal implant devices for retinal implants, with the aim to restore the sight of people who have lost their vision and visual acuity (VA) to better than blindness level. In light of the electronic device simulator, the authors present a design depicting the configuration of a high-efficiency NPDA device by incorporating organic nanomaterials. The present researchers' simulated NPDA device embeds 3600 stimulating pixels (100 μm in diameter) dispersed over a 5.5-mm active radius area. By optimizing the NPDA device geometry, authors demonstrated that each pixel has the potential to produce the required electrical current and voltage for neuronal stimulation utilizing an irradiance of 12 mW/mm^2. Here, the authors concentrated on increasing the efficiency of the device because the increase in efficiency will tend to result in more pixels (greater number of electrodes by reducing the electrode geometry) if the increase in a pixel increases the visual perception. Therefore, theoretically, the 100-μm Tin electrode can reinstate VA up to 20/80. This NPDA implant has the potential to reinforce vision to a level of VA that is superior to that of the vision loss level.

Introduction

Mokwa (2008) demonstrated that retinal degeneration is one of the causes of visual impairment in developed countries. The most common causes of visual impairment or vision loss are age-related macular degeneration (AMD) and retinitis pigmentosa (RP). BrightFocus Foundation recently reported that macular degeneration is a leading cause of global visual impairment (Rein, 2009). It primarily affects people over the age of 60 and the elderly. According to Wong et al. (2014), there are currently 196 million individuals affected by macular degeneration worldwide, which is expected to increase to 288 million by 2040. In a 2004 study, Congdon et al. reported that individuals affected by AMD and RP have a visual acuity (VA) of 20/200, the legal blindness range. Available treatments are ineffective against these retinal disorders, which cause cells in the retina to stop functioning and ultimately die. The majority of the studied cases indicated that a few of the retinal ganglion cells (RGCs) remain working even after AMD or RP screening is sufficient for restoring vision (Mokwa, 2008). Brindley & Lewin (1968) were among the first to attempt to design a visual prosthesis for blind persons that stimulated the visual brain directly. Using a technological implant to bypass non-functioning rods and cones or the optic nerve, these patients may be able to regain some vision.

Restoring vision to patients influenced by these retinal disorders has prodded the advancement of retinal implants worldwide. This has propelled numerous research groups to investigate the efficacy of extracellular electrical stimulation to restore some vision by either epiretinal or subretinal implant approaches. Humayun et al. (2012) later tested the Argus II retinal prosthesis device in blind people with acute outer retinal degenerative diseases. These epiretinal implants restore vision up to a VA of 20/1260. Zrenner et al. (2010) later reported the device composed of 1500 working micro photodiodes describes the subretinal micro photodiode array (MPDA) with 1500 photodiodes may provide a precise significant sense of sight VA of 20/546 in previously blind individuals. As a result, restoring vision beyond the level of visual impairment might be a massive phenomenon in retinal implant performance. Lorach et al. (2015) demonstrated that micro photodiodes for subretinal implant, composed of up to 1500 photodiodes in a 1- to 3-mm device with a pixel width of 70 μm, which was implanted in the photoreceptor region where photoreceptor cells were affected, stimulates retinal neurons in rats in a highly localized manner. The range of the electrical signals measured in retinal cells matched that of the natural visual receptive fields. Watterson et al. (2017) proposed a novel device that mimics the neurons' fractal

Prof. VIRANJAY M. SRIVASTAVA (M'09, SM'13) is a Doctorate (2012) in the field of RF Microelectronics and VLSI Design, Master (2008) in VLSI design, and Bachelor (2002) in Electronics and Instrument-ation Engineering. He has worked on the fabrication of devices and the development of circuit design. Presently, he is working in the Department of Electronic Engineering, Howard College, University of KwaZulu-Natal, Durban, South Africa. He has more than 20 years of teaching and research experience in the area of VLSI design, RFIC design, and Analog IC design. He has supervised various Bachelors, Masters and Doctorate theses.

Prof. Srivastava is a Professional Engineer of ECSA, South Africa, and Life member of IEEE-HKN, Senior members of IEEE, SAIEE, and members of IET, IITPSA. He has worked as a reviewer for several Journals and Confer-ences, both national and international. He is the author/co-author of more than 300 scientific contributions, including articles in international refereed Journals and Conferences, and also the author of various books.

shape. The simulation studies showed how fractal properties interact to produce enhanced stimulation. For the first time, patients will be able to see with the VA required to navigate spaces and roads. A conventional implant architecture for the subretinal implant comprises the silicon-based device, which has many pros and cons that the authors have previously reported. Nowadays, organic nanomaterials and conjugated polymers play a vital role in developing bio-devices; because of their unique properties, they attract researchers to move from conventional silicon-based devices to these organic-material-based bio-devices.

Recently, Ferlauto et al. (2018) and Vagni et al. (2022) created POLYRETINA, a flexible and optoelectronic-based epiretinal prosthesis that helps to stimulate wireless RGCs. They revealed that POLYRETINA is foldable, with 2215 stimulating pixels within a focal length of 46.3 degrees, 967 of which are in the focal area of 5 mm. It demonstrates substantial progress toward enhancing the visual field and VA with the same device, which is currently a difficult challenge for researchers. However, there are some drawbacks of previously reported works. To overcome those issues, Moorthy et al. (2019) recently reported bulk hetero junction (BHJ)-based nano photodiode array (NPDA)—utilizing organic photodiodes, featuring a graphene/semiconducting single-wall carbon nanotube (s-SWCNT/C_{60})/aluminum (Al) pattern, and featuring 1600 electrodes (Figure 1)—as the ideal solution to this problem. The authors evaluated design optimization and developed and tested an NPDA device using conjugated polymers and nanomaterials to restore sight to patients blinded by degenerative retinal diseases in this work. BHJ-based technology created NPDA for subretinal stimulation. Each pixel comprises a graphene bottom anode, an s-SWCNT/C_{60} blend, and a top cathode made of aluminum with a diameter of 100 μm or 150 μm. This NPDA device photovoltaically transforms incident light into an electric current to stimulate nearby photoreceptor neurons without using an external power supply.

The fabricated device has a photo-current density of 245 μA/cm^2 and a photo-voltage of 0.31 V. These findings indicate that the BHJ cell utilizing the photodiode array used in this research work outperforms previously reported work. The significant improvement in photovoltaic performance paved the way for the density of the NPDA array in the prostheses to be scaled up. An increased number of electrodes will improve VA to a more significant extent. The authors previously reported a comparative evaluation of PHJ and BHJ nano photodiodes (NPDs). They evaluated the performance and viability of effectively implementing such a device for subretinal implantable devices to evaluate the impact of the BHJ-based NPD (Moorthy et al., 2018). The objective of the work was to model a multi-disciplinary (multi-physics) organic photovoltaic (OPV) by using mathematical modeling and analyzing the behavior of a standard planar heterojunction. Results show that the performance of organic solar cells is sensitive to the thickness of the photoactive substance (Moorthy et al., 2022).

This work mainly focuses on comparing the PHJ and BHJ NPDs for various geometries and optimizing the design to achieve the performance suitable for human subretinal implants. The previous work found that the comparison results on PHJ and BHJ NPD device parameters clearly show that BHJ NPD performance is much better than PHJ NPD in all aspects. The findings suggested the potential that a single photodiode may be used to stimulate the retina. Whereas the silicon MPDA model might necessitate two or more photodiodes wired in series to provide the required voltage, contemporary versions employ three photodiodes (Mathieson et al., 2012). The consequential order of magnitude reduction in pixel size for BHJ-based NPDA retinal implants was expected to influence VA and visual field significantly. The NPDA implant has the potential to provide 20/80 vision, allowing for the first time the restoration of vision to the level necessary for ambulatory tasks. The authors also suggested that the increased number of pixels (due to the reduction in electrode diameter trying to promote more neural stimulus) and the favorable optoelectronic properties (such as incredible transmission in which the mediated illuminance is higher than that predicted from a simple pixel count of the photodiode's exposed area), as well as an increase in mechanical systems, could all benefit from this NPDA configuration (which could be used to enable a less invasive surgical procedure and make it possible for devices to conform to the curved surface just at the back of the eye). Five patients with geographic atrophy were implanted with a wireless 2 × 2-mm-wide, 30-μm-thick device having 378 pixels of 100 μm in size. All five patients achieved the work's primary outcome by demonstrating the prosthetic visual perception in the former scotoma (Palanker et al., 2022).

Figure 1.
(a) Fabricated and (b) schematic view of the NPDA device. NPDA, nano photodiode array.
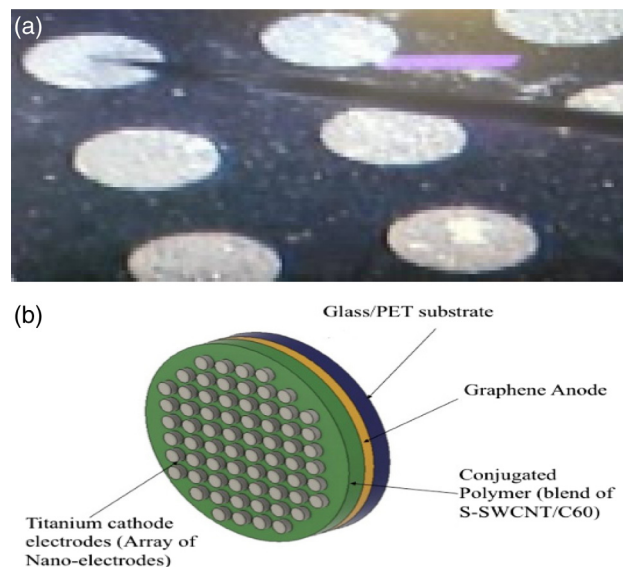
A few modeling and simulation studies on retinal implant devices have been performed to analyze the performance and efficiency of the MPDA, which found that the performance of the device is sufficient to stimulate the retinal neurons in both simulation and real time. However, after 9 months, the MPDA subretinal implant developed degradation (Mathieson et al., 2012). Eventually, because the MPDA was built on solid silicon (Si) substrates, the implantation of such devices has been challenging. To address this issue, preliminary steps were taken in developing an overall system for modeling retinal prostheses in the current work to evaluate the aspects that influenced the efficiency and performance of the device required to stimulate the photoreceptors. Discerning photodiode voltage and photodiode current density are critical for accomplishing invulnerable stimulation. Device performance, along with electrode geometry, is an appropriate factor that influences retinal stimulation. An improved integrated simulation configuration can predict stimulation parameters by incorporating these components into the model. The performance of the retinal device contributed significantly to the differing current spread from the electrodes, resulting in changes in the stimulus area in the retina and thus affecting the prosthesis's pixel density. In vitro, electrophysiological data and analyses imply that increasing the device's efficiency increases resolution.

The authors designed a framework to simulate the NPDA device for subretinal implants in this research. Variations in photodiode currents and voltage were derived using this structure with different electrode sizes, geometries, and illumination. To illustrate the significance of this current simulation model to implanted human retinal prostheses, the results collected from the present simulation model are constructed by the most recent experimental data provided in polyretina and NPDA devices. The main objective was to propose a numerical framework that would allow us to optimize our device to design a more efficient and safe retinal prosthesis. In this research, the authors have presented the simulation models chosen for representing living matter, and current and voltage measurements are performed to assert the validity of those choices. As a result, this simulation model is easily adaptable to predicting newer electrode configurations' efficacy for subretinal prosthetic devices. Compared to the previously reported implants, the NPDA design is best to activate all the neighboring cells—other electrode devices need too much irradiation. NPDA implants will not require supplemental infrared radiation to be beamed into the eye because natural light is sufficient to stimulate. Furthermore, the authors showed that the 50-μm electrode size NPDA implant has the potential to deliver a maximum VA of 20/80. The authors also cover various strategies for lowering irradiance requirements. This paper has been organized as follows. Section 2 focuses on the modeling and methodology used in this work

and sample preparation for experimental analysis. Section 3 realizes the numerical simulations and discussion. Section 4 describes the results and analysis of the research. Finally, Section 5 concludes the work and recommends future areas of research.

Modeling and Methodology

The NPDA array using nanomaterials has been modeled and simulated using electronic device simulator (EDS) tools. The results obtained for these structures are compared to optimize the device dimensions of NPDA devices with better performance. The sun's light strikes the glass first, then passes through a 50-nm-thick transparent conductive electrode, graphene, and a 100-nm-thick active layer, s-SWCNT/C_{60} (Moorthy et al., 2022). The last layer is a titanium-based metal electrode with a thickness of 100 nm. The electrode size, the electrode density, the active layer thickness, and the anode layer thickness. To test the device's functionality, certain parameters will be varied. Figure 1(a) shows a proposed NPDA device design's simulation structure for a subretinal photodiode. The incident photon will generate electron-hole pairs in the presence of light. These pairs of electrons will be collected and transferred to the electrode cathode array via photodiodes. The optical power absorbed per unit volume in such a photoactive layer in contexts of the index and electric fields can be expressed as

$$P_{abs}(r, \lambda) = -\frac{\omega}{2} * |E(r, \lambda)|^2 * Im(\varepsilon(r, \lambda)) \tag{1}$$

where P_{abs}, E, and ε are the wavelength and position-dependent absorbed power, electric field, and material permittivity, respectively. The position-dependent generation rate accounting for a given wavelength, G(x, λ), can be easily determined by dividing the absorption power by the photon energy for each λ:

$$G(r, \lambda) = -\frac{\pi}{h} * |E(r, \lambda)|^2 * Im(\varepsilon(r, \lambda)) \tag{2}$$

Eventually, the position-dependent generation rate for broad-spectrum sunlight (AM 1.5G) can be determined by finding G (x, λ) over the spectral range:

$$G(r) = \int G(r, \lambda) d\lambda \tag{3}$$

When there is no recombination attributed to the charge, the short-circuit current density is calculated from optical simulation using the generation rate profile during the collection process:

$$J_{SC} = \frac{e \int G(r) dr}{A} \tag{4}$$

where J_{sc} is the short-circuit current density, e is the electron charge, and A is the unit cell area (simulation region). To calculate P_{abs}, G(r), and J_{sc} of only the active material in different simulation setups. s-SWCNT/C_{60} and optimized graphene refractive index characteristics (thermally annealed) and developed designs were given as input variables to the software.

The electrodes' geometries were optimized to find the optimal model parameters that resulted in the best stimulation selectivity. When a collection of design variables generated the highest current concentration in the target of stimulus, the electrode geometry was deemed optimal. Figure 2(a) shows the schematic view of the proposed NPDA device model for subretinal implant designed using the EDS tool, and Figure 2(b) shows that the NPDA device features a flexible substrate, a bottom electrode graphene, a blend of semiconducting layer (s-SWCNT/C_{60}), and the top electrode (Tin).

Numerical Simulations and Discussion

The main focus of this work is to optimize NPDA device geometries to achieve performance suitable for human subretinal implants. The OPV-based NPDA using nanomaterials has been modeled and simulated using the finite-difference time-domain (FDTD) solver (Lumerical Solutions, Inc.). The results obtained for these structures are compared to optimize NPDA device dimensions for better

Figure 2.
(a) Schematic view of the proposed NPDA device and (b) illustration of NPDA device stimulating neurons extracellularly. NPDA, nano photodiode array.
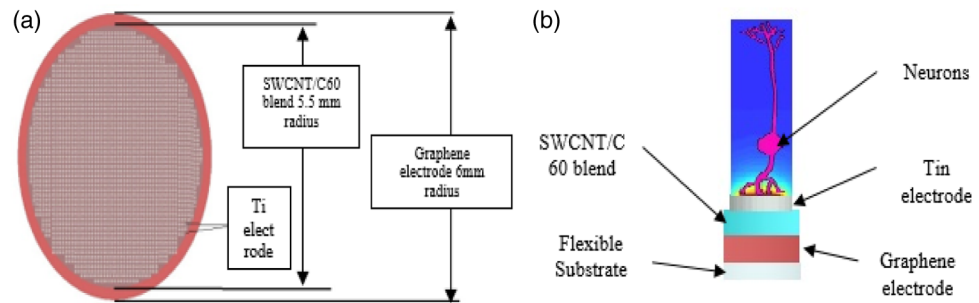
performance. This design aims to identify the best configurations and parameters for producing the highest current densities in the stimulus target.

The proposed model simulated in this research is depicted in Figure 2(b). Large area manufacturing is possible due to its light weight, cheap cost, flexibility, and solution-based nature; a quintessential polymer photovoltaic solar architecture is used as a testing platform for understanding the impact of the light absorption of the active material (Ganguly et al., 2020; Ganguly & Srivastava, 2021). The top cathode layer, Ti electrode structures are organized in circular lattices regularly. The space between successive structures is maintained constant at 100 nm. The structures are simulated from this perspective. The metal constructions are composed of a circle with a radius R mounted on a cylindrical pillar with radiuses varying from 50 to 150 μm (Srivastava & Singh, 2014; Gowthaman & Srivastava, 2022). A plane wave traveling in the z-direction with the AM 1.5G spectra in the range of 300 nm to 1400 nm is used to replicate sunlight. The FDTD solution is utilized for numerical computations. Whereas the refractive index is constant, the dielectric constants for graphene, s-SWCNT/C_{60}, and Ti are dispersive and complex.

The geometries were simulated using an AM 1.5G spectrum with wavelengths ranging from 300 nm to 1400 nm. The active material s-SWCNT/C_{60} mix has significant absorption spectra between 300 and 650 nm, whereas the active layer exhibits effective spectra between 800 and 1300 nm. The AM 1.5G optical spectra from 300 nm to 1300 nm were employed to excite the unit cells. Without computing Poisson's equations, J_{sc} may be determined using optical simulations (Eq. 4). The thickness of the active layer also influences the recombination process. Because carrier recombination is not insignificant in thicker BHJ, the authors are focused on comparatively thin films; therefore, the thickness of active materials has been changed from 50 nm to 200 nm. Beyond this thickness, recombination takes over, and the estimation of J_{sc} based on the generation rate is no longer valid.

Figure 3 shows the absorption spectra of the s-SWCNT/C_{60} blend active layer with different thicknesses. As is evident from the absorption spectra shown in Figure 3, after 800 nm, the device absorbs near infrared (NIR) light, and the spectra are increased when the thickness of the film increases; this is because of the high absorption of light.

Results and Discussion

In this research, anode layer thickness (graphene) is compared between 20 nm and 50 nm, with active layer thicknesses varying from 50 nm to 200 nm while cathode layer thicknesses are maintained at 50 nm in the normal illumination range and the NIR range.

Figure 4 illustrates the comparison plot of different anode layer thicknesses versus J_{sc} for 20-nm and 50-nm graphene layer thickness with the illumination range of 100 mW/mm². The J_{sc} from optical simulation varies depending on the simulation model's or actual material's simulation range, recombination, and refractive index. For a solar cell with different thicknesses, an improvement in

Figure 3.
Absorption spectra of S-SWCNT/C₆₀ blend active layer with different thicknesses. a.u., arbitrary units.
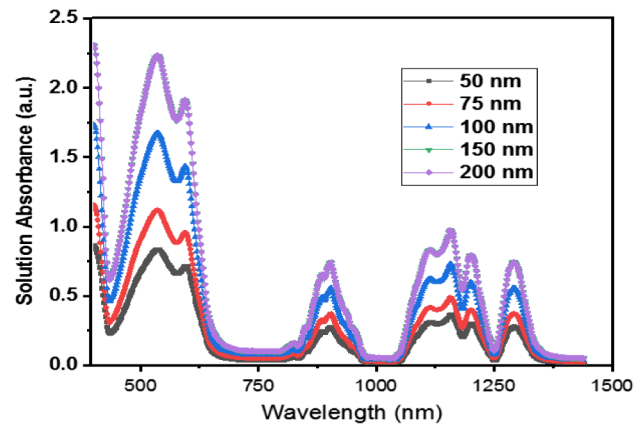
Figure 4.
J_{sc} comparison plot of 20-nm and 50-nm graphene layer thickness for different anode layer thickness vs. short circuit current density with the illumination of 100 mW/mm². J_{sc}, short-circuit current density.
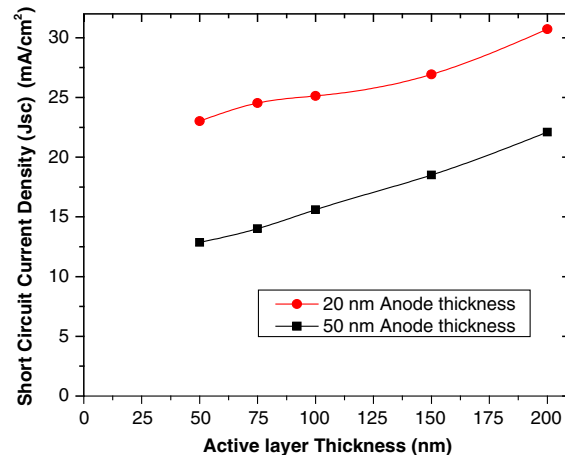
J_{sc}, open-circuit voltage (V_{oc}), and efficiency has been observed in the cases of 20-nm and 50-nm graphene electrode thicknesses.

Even though the NPDA device absorbs more NIR light, studies have shown that the latter has a higher J_{SC}, with J_{SC} values ranging between 200 and 700 µA/cm² for both the 20-nm and 50-nm graphene layer thickness, respectively. Figures 4 to 9 show that 20-nm graphene layer thickness shows better performance when compared to 50 nm in all parameters; the increase in active layer thickness will increase the device's performance in both cases.

The authors used the power absorption spectra for the s-SWCNT/C₆₀ solar cell at various blend thicknesses to illustrate the cause of such oscillating characteristics in the photo-current density versus thickness. As thickness increases, increased power from higher wavelengths is absorbed, as seen in Figure 3. This enhances the overall absorbance across the spectrum. According to the facts given earlier, there is a thickness at which the combined impact of charge creation, transit, and

Figure 5.
V_{oc} comparison plot of 20-nm and 50-nm graphene layer thickness for different anode layer thickness vs. short circuit current density with the illumination of 100 mW/mm². V_{oc}, open-circuit voltage.
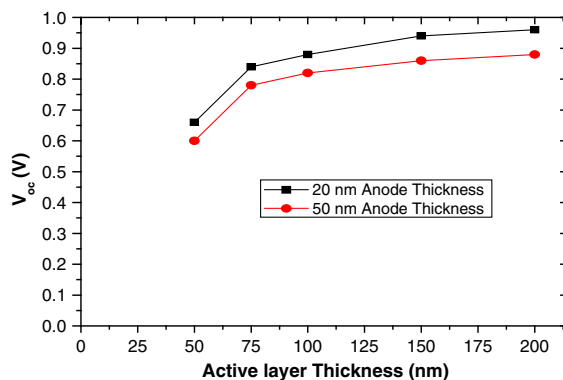

Figure 6.
Comparison plot anode layer thickness vs. efficiency for 20-nm and 50-nm graphene layer thickness with the illumination of 100 mW/mm².
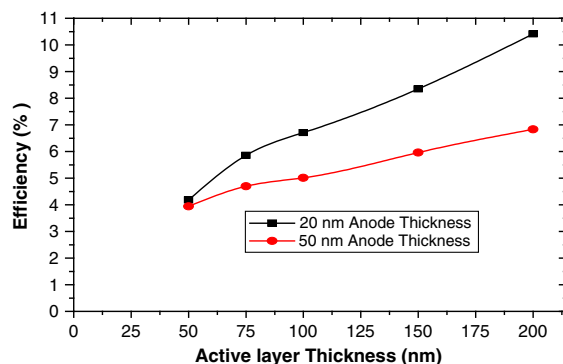

Figure 7.
J_{sc} comparison plot of 20-nm and 50-nm graphene layer thickness for different anode layer thickness vs. short circuit current density with the NIR illumination. J_{sc}, short-circuit current density; NIR, near infrared.
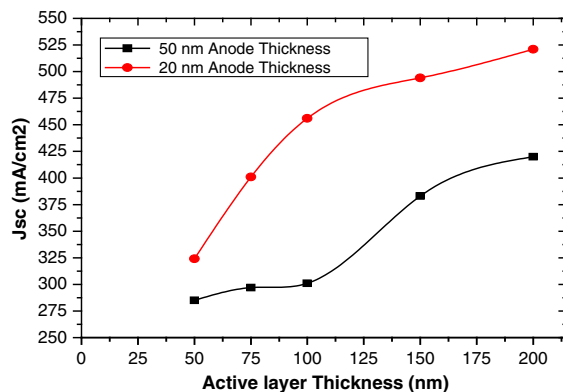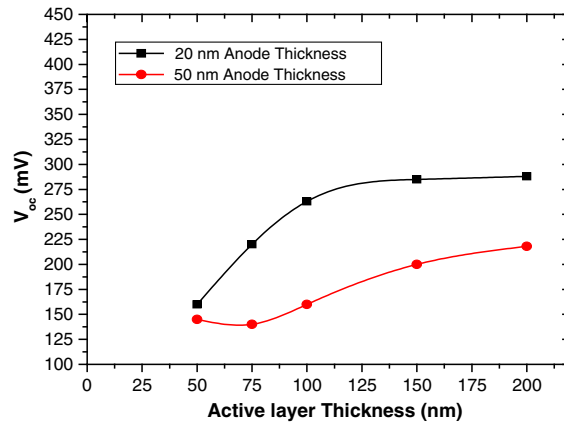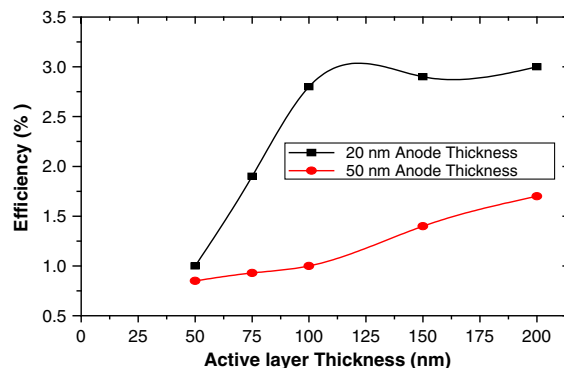
collection achieves an optimum, and the device's efficiency is improved. The authors are interested in researching the effect of layer thickness on J_{sc} and V_{oc} of active materials. Essentially, V_{oc} directly indicates the active layer's built-in potential (V_{bi}). Because V_{bi} remains constant across all thicknesses, V_{oc} remains relatively constant. Because of the proportional relationship, the variation of J_{sc} with thickness follows a similar pattern to efficiency. In both cases, under normal illumination range and NIR, the 20-nm graphene layer device is superior to the 50 nm because of the excellent absorption and high light transmittance. When the thickness of the active layer is raised from 50 nm to 200 nm and the thickness of the graphene layer is 20 nm, the improvement is 66 %. The graphene layer with 20 nm absorbs more light than the graphene layer with 50 nm.

The authors developed the research by changing the cathode pillar dimension and calculating the photo-current within a particular range. The authors considered the pillar electrode size to be between 50 μm to 150 μm, the height 50 nm, and the step size 50 nm. Figures 9 and 10 show the resultant photo-current and photo-voltage.

The photo-current and photo-voltage of a 50-nm-tall pillar first decrease with increasing pillar diameter and have their maximum at 50 nm, and the increase in electrode size decreases the performance.

Figure 10.
Photo-current density with the NIR illumination for various cathode electrode sizes. NIR, near infrared.
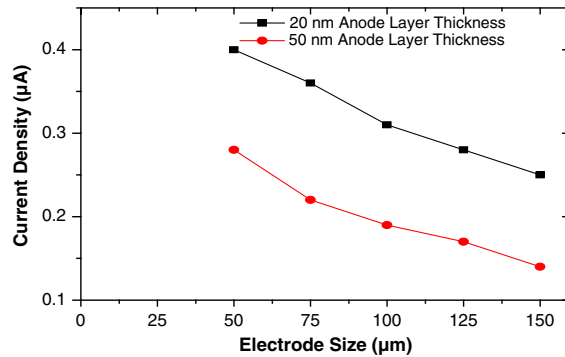

As a result, for a 100-nm s-SWCNT/C_{60} active layer, a pillar structure with a height of 50 nm and a radius of 50 nm will be optimal for the subretinal implant. Figures 10 and 11 show the photo-current and photo-voltage generated by various cathode electrode geometries.

Figures 4 to 11 illustrate how the device's parameters vary with changes in active layer thickness, anode layer thickness, and cathode electrode dimensions under AM 1.5G and NIR illumination settings. The authors did not include any resistance in the contact areas in this work. As a result, photovoltaic parameter values deviate somewhat from experimental values. The efficiency of this device with the standard design was greater than that of other active materials evaluated in the previously reported research. The best active layer thickness has also been identified as 100 nm, sufficient for retinal implant application.

The aforementioned analysis and comparison of results on various parameters of NPDA and the optimum layer thicknesses and cathode electrode geometries for maximizing performance are realized on a flexible substrate, graphene layer with a thickness of 50 nm, s-SWCNT/C_{60} with a thickness of 100 nm as a photoactive layer, and titanium (Ti) electrodes with a thickness of 100 nm. The device's size is modeled as 6-mm radius (r) with an active area of 5.5 mm r. Under these conditions, the decrease in electrode size will increase the performance. Concerning VA, with an electrode size of 50 µm, VA restored by NPDA is in the order of 20/80, which is better than the current retinal prostheses. Nevertheless, because these calculations are based on numerical simulations, they should be verified in vivo in animals and individuals. Furthermore, because the

Figure 11.
Photo-voltage with the NIR illumination for various cathode electrode sizes. NIR, near infrared.
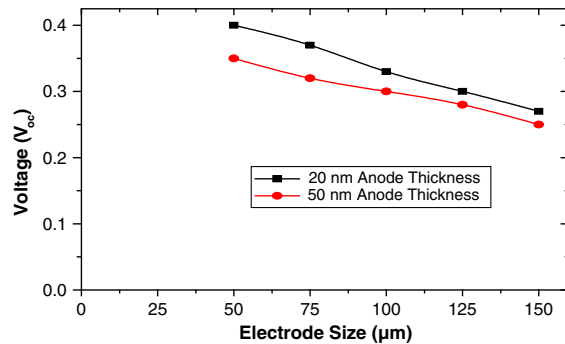
pixel size is reduced, the photo-current produced by the interface is reduced, the performance of stimulating RGCs should be reevaluated.

Conclusion and Future Recommendations

The authors modeled, optimized, and compared the results of various parameters including open V_{oc}, J_{sc}, fill factor, and efficiency for optimizing the NPDA device for subretinal implant by improving the VA and visual field under different illumination conditions. This design has been carried out by varying the thicknesses of the anode, cathode electrode size, and active layers. The obtained results have concluded that 20-nm graphene layer thickness device performance is better than that of the 50-nm device in all parameters, such as efficiency of V_{oc}, J_{sc}, fill factor, and efficiency at both irradiance levels. Furthermore, the 50-µm cathode electrode size device shows better performance compared to others. Moreover, the authors have demonstrated a technique for improving the performance of an NPDA device using Ti nano pillar structures incorporated in the NPDA. This work aims to optimize the NPDA device structure and geometries to maximize the subretinal implant's photodiode array performance.

By improving the performance of the NPDA device, one can achieve a higher VA and visual field of the subretinal device. The future NPDA device should be realized in soft/flexible substrate with more stimulating electrodes, which improves the VA and visual field. The fabricated NPDA device will be tested both in vivo and in vitro.

References

Brindley, G. S., & Lewin, W. S. (1968). The sensations produced by electrical stimulation of the visual cortex. *The Journal of Physiology*, *196*(2), 479–493. https://doi.org/10.1113/jphysiol.1968.sp008519

Congdon, N., O'Colmain, B., Klaver, C. C., Klein, R., Muñoz, B., Friedman, D. S., Kempen, J., Taylor, H. R., & Mitchell, P. (2004). Causes and prevalence of visual impairment among adults in the United States. *Archives of Ophthalmology*, *122*(4), 477. https://doi.org/10.1001/archopht.122.4.477

Ferlauto, L., Airaghi Leccardi, M. J., Chenais, N. A., Gilliéron, S. C., Vagni, P., Bevilacqua, M., Wolfensberger, T. J., Sivula, K., & Ghezzi, D. (2018). Design and validation of a foldable and photovoltaic wide-field epiretinal prosthesis. *Nature Communications*, *9*(1). https://doi.org/10.1038/s41467-018-03386-7

Ganguly, A., & Srivastava, V. M. (2021). *Improved efficiency in solar cells using Fe doped ZnS quantum dots as sensitizers* [presentation]. 16th IEEE IST-Africa Week Conference (IST-Africa Institute), Durban, South Africa, 1–9.

Ganguly, A., Nath, S. S., & Srivastava, V. M. (2020). Enhanced efficiency in swift 100 MeV Ni ion irradiated Zns quantum dot sensitized solar cell. *Chalcogenide Letters*, *17*(10), 487–493.

Gowthaman, N., & Srivastava, V. M. (2022). Mathematical modeling of drain current estimation in a CSDG MOSFET, based on La2O3 oxide layer with fabrication—A Nanomaterial approach. *Nanomaterials*, *12*(19), 3374. https://doi.org/10.3390/nano12193374

Humayun, M. S., Dorn, J. D., Da Cruz, L., Dagnelie, G., Sahel, J., Stanga, P. E., Cideciyan, A. V., Duncan, J. L., Eliott, D., Filley, E., Ho, A. C., Santos, A., Safran, A. B., Arditi, A., Del Priore, L. V., & Greenberg, R. J. (2012). Interim results from the international trial of second sight's visual prosthesis. *Ophthalmology*, *119*(4), 779–788. https://doi.org/10.1016/j.ophtha.2011.09.028

Lorach, H., Goetz, G., Smith, R., Lei, X., Mandel, Y., Kamins, T., Mathieson, K., Huie, P., Harris, J., Sher, A., & Palanker, D. (2015). Photovoltaic restoration of sight with high visual acuity. *Nature Medicine*, *21*(5), 476–482. https://doi.org/10.1038/nm.3851

Mathieson, K., Loudin, J., Goetz, G., Huie, P., Wang, L., Kamins, T. I., Galambos, L., Smith, R., Harris, J. S., Sher, A., & Palanker, D. (2012). Photovoltaic retinal prosthesis with high pixel density. *Nature Photonics*, *6*(6), 391–397. https://doi.org/10.1038/nphoton.2012.104

Mokwa, W. (2008). Artificial retinas. *Comprehensive Microsystems*, 201–217. https://doi.org/10.1016/b978-044452190-3.00027-6

Moorthy, V. M., Daniel, R. J., & Shanmugaraja, P. (2018). Comparison studies of planar and bulk hetero junction nano photo diodes using carbon nano tube's (CNT) and graphene for sub-retinal implant. 2018 Conference on Emerging Devices and Smart Systems (ICEDSS), Tiruchengode, India. https://doi.org/10.1109/icedss.2018.8544352

Moorthy, V. M., Sugantharathnam, M., Rathnasami, J. D., & Pattan, S. (2019). Design and characterisation of graphene-based nano-photodiode array device for photo-stimulation of subretinal implant. *Micro & Nano Letters*, *14*(11), 1131–1135. https://doi.org/10.1049/mnl.2019.0030

Moorthy, V. M., Varatharajan, P., Rathnasami, J. D., & Srivastava, V. M. (2022). G-optrode bio-interfaces for non-invasive optical cell stimulation: Design and evaluation. *Biosensors*, *12*(10), 808. https://doi.org/10.3390/bios12100808

Palanker, D., Le Mer, Y., Mohand-Said, S., & Sahel, J. A. (2022). Simultaneous perception of prosthetic and natural vision in AMD patients. *Nature Communications*, *13*(1). https://doi.org/10.1038/s41467-022-28125-x

Rein, D. B. (2009). Forecasting age-related macular degeneration through the year 2050. *Archives of Ophthalmology*, *127*(4), 533. https://doi.org/10.1001/archophthalmol.2009.58

Srivastava, V. M., & Singh, G. (2014). *MOSFET technologies for double-pole four-throw radio-frequency switch* [Analog Circuits and Signal Processing series]. Springer. https://doi.org/10.1007/978-3-319-01165-3

Vagni, P., Airaghi Leccardi, M. J., Vila, C., Zollinger, E. G., Sherafatipour, G., Wolfensberger, T. J., & Ghezzi, D. (2022). Polyretina restores light responses in vivo in blind gottingen minipigs. *Nature Communications*, *13*(1). https://doi.org/10.1038/s41467-022-31180-z

Watterson, W. J., Montgomery, R. D., & Taylor, R. P. (2017). Fractal electrodes as a generic interface for stimulating neurons. *Scientific Reports*, *7*(1). https://doi.org/10.1038/s41598-017-06762-3

Wong, W. L., Su, X., Li, X., Cheung, C. M., Klein, R., Cheng, C., & Wong, T. Y. (2014). Global prevalence of age-related macular degeneration and disease burden projection for 2020 and 2040: A systematic review and meta-analysis. *The Lancet Global Health*, *2*(2), e106–e116. https://doi.org/10.1016/s2214-109x(13)70145-1

Zrenner, E., Bartz-Schmidt, K. U., Benav, H., Besch, D., Bruckmann, A., Gabel, V., Gekeler, F., Greppmaier, U., Harscher, A., Kibbel, S., Koch, J., Kusnyerik, A., Peters, T., Stingl, K., Sachs, H., Stett, A., Szurman, P., Wilhelm, B., & Wilke, R. (2010). Subretinal electronic chips allow blind patients to read letters and combine them to words. Proceedings of the Royal Society B: Biological Sciences, *278*(1711), 1489–1497. https://doi.org/10.1098/rspb.2010.1747